Passive Mode-Locking in AlGaInAs 1.55-μm Strained Quantum Well Lasers: Modeling and Experiment

J. Javaloyes[(1)], P. Stolarz[(1)], L. Hou[(1)], M. Sorel[(1)], A.C. Bryce[(1)], S. Balle[(2)]

[(1)] Department of Electronics and Electrical Engineering, University of Glasgow, Glasgow, G12 8LT, United Kingdom, ✉ julien.javaloyes@elec.gla.ac.uk
[(2)] Institut Mediterrani d'Estudis Avançats (IMEDEA), CSIC-UIB, C/ M. Marques, 21, 07190 Esporles, Spain.

Abstract *We study the Mode-Locking dynamics of 40-GHz semiconductor Fabry-Pérot lasers with intracavity saturable absorber by using a Traveling-Wave-Model and a time-domain response of the semiconductor material. We analyze the influence of key parameters and compare our predictions with experimental results.*

Introduction

Mode-locking (ML) of lasers is a subject of intense research both theoretically and experimentally. The theoretical challenge arises from the complex nonlinear dynamics involving the self-organization of many laser modes while the experimental motivation comes from the large number of applications of short pulse sources in medicine, metrology and telecommunications[1]. ML has led to the shortest and most intense optical pulses ever generated. Semiconductor mode-locked lasers have the added attraction of being compact, low cost and adaptable to many cavity geometries[2].

Haus' master equation[1] is a widely used approach to study passive mode-locking in the time domain. Analytical predictions on the pulse properties can be assessed under the assumption of weak saturation. However, even if pulse iterative models have provided some useful insight into the mode-locking problem, these approaches when applied to a particular design provide only a qualitative predictions, due to the many simplifying hypothesis involved. On the other hand, approaches based on finite difference time domain description[3] of the electromagnetic field and the semiconductor Bloch equations description of the active medium[4], require enormous computational power which impede parametric studies.

To circumvent these limitations and shed some light onto the mode-locking scenario, we describe the dynamics of the device by resolving the propagation of the electromagnetic waves under the Slowly-Varying-Approximation. The light-matter interaction is described by means of a frequency-domain analytical approximation to the optical susceptibility[5] that we recently transformed into a time-domain description[6]: Our approach provides important spectral features usually disregarded as for instance the abrupt spectral variations of the absorption in the saturable absorber. However, the effectiveness of our approach still allows for parametric studies: a typical 125 ns simulation run[7] is achieved in 15 minutes on a standard PC. As such our model allows for the construction of bifurcation diagrams.

Model

We shall consider a Fabry-Pérot cavity divided in two sections. The first one, from $z = 0$ to $z = 1-l$ is electrically pumped and corresponds to the amplifier section; the second one, from $z = 1-l$ to $z = 1$, corresponds to a saturable absorber (SA) section of relative length l. We consider that there is no reflectivity at the amplifier-SA interface, and that the cavity is defined by simple cleaved facets, i.e. $r \simeq 30\%$.

Within each section, the slowly-varying amplitudes of the forward and backward waves[8], $E_{\pm}(z,t)$, evolve according to

$$\begin{aligned}
(\partial_t \pm \partial_z) E_{\pm} &= i\Gamma P_{\pm} - \alpha_i E_{\pm} , && (1)\\
\partial_t N_0 &= J - R(N_0) \\
&- i\left(P_+ E_+^{\star} + P_- E_-^{\star} - c.c.\right), && (2)\\
\partial_t N_{\pm 2} &= -\left(R'(N_0) + 4\mathcal{D}q_0^2\right) N_{\pm 2} \\
&- i\left(P_{\pm} E_{\mp}^{\star} - E_{\pm} P_{\mp}^{\star}\right), && (3)
\end{aligned}$$

where α_i are the internal losses of the system, Γ is the optical confinement factor, and for numerical purposes we have scaled time and space to the cavity transit time and to the optical length of the cavity, respectively. J is the current density injected per unit time (normalized to the electron charge) into the section and $q_0 = (2\pi n_g)/\lambda$ is the optical carrier wavevector. The recombination is assumed to be of the form $R(N) = AN + BN^2 + CN^3$ where A, B and C are the non radiative, bi-molecular and Auger recombination coefficients, respectively. In addition, $N_0(z,t)$ is the quasi-homogeneous component of the spatially dependent, time evolving carrier density, $N_{+2}(z,t) = N_{-2}^{\star}(z,t)$ is the complex ampli-

978-1-4244-8535-2/10/$26.00 ©2010 IEEE

tude of the carrier density grating at half the wavelength which is generated by the presence of the two counter-propagating waves and $\mathcal{D}$ is the ambipolar diffusion coefficient. We assume that the SA is reverse biased and presents a sweep out rate of the carriers A_{SA} much larger than in the gain section A_G.

The closure of our model is achieved by providing the link between the polarization and field amplitudes according to[6]

$$\begin{gathered} P_{\pm}(z,t) \\ = \\ \int_0^{\infty} \tilde{\chi}\left[s, N_0(z,u)\right] E_{\pm}(z,u) ds \\ + \\ \int_0^{\infty} N_{\pm 2}(z,u) \frac{\partial \tilde{\chi}}{\partial N}\left[s, N_0(z,u)\right] E_{\mp}(z,u) ds \end{gathered} \tag{4}$$

where $u = t - s$, and $\tilde{\chi}(s, N)$ is the Fourier transform of the frequency-dependent susceptibility of the active material found in[5], and reads

$$\begin{gathered} \tilde{\chi}(s,N) \\ = \\ \chi_0 s^{-1} e^{-(\gamma_{\perp} + i\Omega)s} \left(2e^{-i\frac{N}{N_t}\gamma_{\perp} s} - e^{-ib\gamma_{\perp} s} - 1\right) \end{gathered} \tag{5}$$

with $\gamma_{\perp}$ the dephasing rate, Ω the bandgap frequency and b the top band frequency.

The partial differential Maxwell equations are numerically solved using an second order algorithm while the convolution is performed using trapezoidal integration, see[6] for details.

Results

We summarize in Fig.1 the various frequency scales present in the problem by representing the imaginary part of the susceptibility in the amplifier and SA sections for different values of the carrier density. The chosen values are smaller in the SA section since it is usually operating below transparency, i.e. $N \leq 1$. Our approach allows for having different references band-edge frequencies in the gain and the absorption sections, i.e. Ω_g and Ω_s and thereby grant the possibility of including the important reverse voltage induced quantum confined stark effect.

In order to assess the operating range and the ML quality and stability, we calculated several bifurcation diagrams as a function of some key parameters[7], e.g. bias current, length and recovery time of the SA and bandgap offset between the gain and the SA section. We used the typical method of numerical continuation: the final solution found for one value of the control parameter is used as an initial condition for the next, slightly different, value of the control parameter.

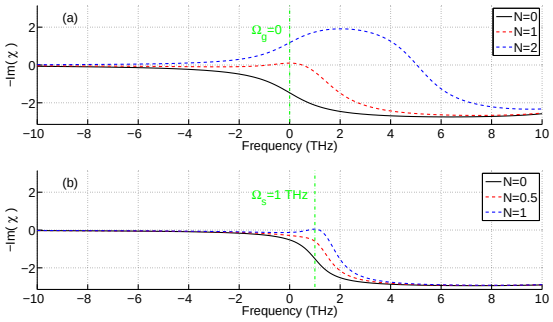

Fig. 1: Gain and absorption in the gain and the SA sections for different values of the carrier density normalized to transparency within each section.

The typical sequence of bifurcations found upon increasing of the bias current is: steady emission, weak multimode dynamics, stable ML, a bubble of Self-Pulsation (SP) if the SA modulation is sufficiently strong and finally a partial degradation of the pulse train for high drive current (ten times threshold).

A similar scenario is also found by varying the length of the SA section for a fixed value of the recovery time $A_{SA}^{-1} = 10$ ps. A full bifurcation diagram is presented in Fig. 3 while Fig. 2 depicts some typical regimes.

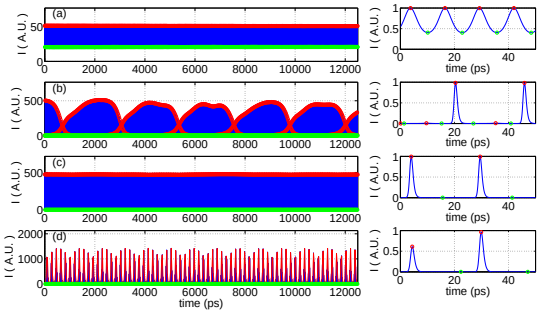

Fig. 2: Long time behavior of the time traces of the field intensity (left) and details of the pulse shape (right). The panels a), b), c) and d) correspond to $l = 1.5\%$, $l = 3\%$, $l = 3.75\%$ and $l = 6.5\%$, respectively

1. For l ranging from 0% up to 1.25% of the cavity length only a weakly multimode dynamics can be seen.
2. For l from 1.5% to 2%, a transition to stable shallow Harmonic ML is found, see Fig.2a) obtained with 1.5%.
3. For l ranging from 2% to 3% unstable ML appears, with substantial modulation of the pulse amplitudes which is accompanied by a considerable jitter as can be seen in the pulse train in Fig.2 b), obtained with $l = 3\%$.
4. For l ranging from 3% to 5% stable ML exists with very low noise triggered jitter, see Fig.2 c) with $l = 3.75\%$.

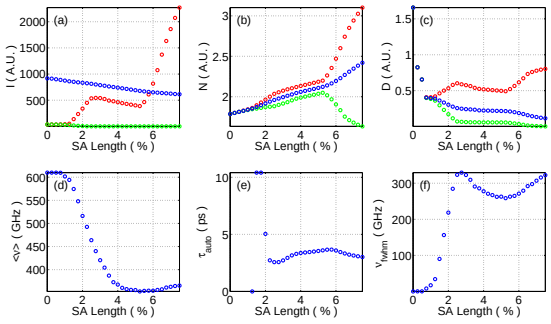

Fig. 3: Bifurcation Diagram as a function of the SA Length, minima, maxima and average values are depicted in green, red and blue, respectively .

5. For l greater than 5.25% the device enters a SP regime, see Fig.2 d) obtained with $l = 6.5\%$.

This phenomenology is in good agreement with the bifurcation map of passively Mode-Locked AlGaInAs 1.55-μm strained quantum well laser[9]. The lasers were fabricated with varying saturable absorber lengths at one side of the chip and a 2.5μm wide and 1170μm long straight ridge waveguide define the laser cavity after cleaving. The modal separation is 37.58 GHz. ML is achieved by reverse biasing the SA section thereby increasing the sweep out rate of the photogenerated carriers. Preliminary studies indicate that a reverse Voltage of -3 Volts corresponds to a sweep out time of 10 ps.

We achieved ML characterization by simultaneous recording of the optical and radio-frequency (RF) spectra as well as second harmonic autocorrelation as seen in Fig. 4.

Fig. 5 shows the current-Reverse Voltage map of a device with $l = 3\%$. A broad range of stable ML is obtained for reverse Voltages between -2.5 and -3.5 Volts and bias current ranging from two to four times threshold. For this value of the SA length, a small region of SP can be seen. The typical pulsewidth is 1.2 ps with a time bandwith product of 0.6.

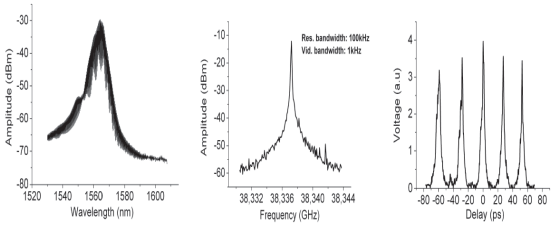

Fig. 4: From left to right : Optical spectrum, RF spectrum and autocorrelation. The current is four times threshold and the reverse voltage is -3 V.

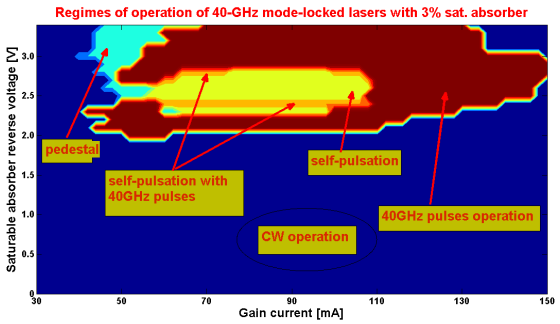

Fig. 5: Experimental operating regime map as a function of the bias current applied to the gain section (horizontal axis) and the reverse voltage applied to the SA section (vertical axis). Blue, light blue, yellow and red indicate no ML, incomplete ML, ML with SP and stable ML, respectively.

Conclusion

The ML dynamics of a semiconductor Fabry-Pérot laser has been explored using a TWM complemented by a new description of the active medium polarization presented in[6]. The effectiveness of our approach allowed us to systematically explore the influence of several important control parameters, and to compare with experimental data. This good qualitative agreement indicates that our modeling approach can be used, upon proper fitting of the material parameters, for optimization of the design of semiconductor ML lasers.

References

1 H. A. Haus, *IEEE J. Selected Topics Quantum Electron.*, vol. 6, pp. 1173–1185, 2000.

2 E. A. Avrutin et al.,*IEE Proc.-Optoelectron.*, vol. 147, pp. 251–278, 2000.

3 K. Yee, *Antennas and Propagation, IEEE Transactions on*, vol. 14, no. 3, pp. 302–307, May 1966.

4 J. Hader et al. *Quantum Electronics, IEEE Journal of*, vol. 35, no. 12, pp. 1878–1886, 1999.

5 S. Balle, *Phys. Rev. A*, vol. 57, pp. 1304–1312, 1998.

6 J. Javaloyes et al. *Phys. Rev. A*, vol. 84, 2010, to appear.

7 J. Javaloyes et al., *Quantum Electronics, IEEE Journal of*, vol. 46, no. 7, pp. 1023–1030, July 2010.

8 L. Narducci et al. *Laser Physics and Laser Instabilities*. Singapore: World Scientific, 1988.

9 L. Hou et al., *Photonics Technology Letters, IEEE*, vol. 21, no. 23, pp. 1731–1733, Dec.1, 2009.